PROCEEDINGS OF SCIENCE

3D silicon sensors: irradiation results

Gian-Franco Dalla Betta[1], **Marco Povoli**
University of Trento and INFN Padova (Gruppo Collegato di Trento)
Via Sommarive, 14 – 38123 Povo di Trento, Italy
E-mail: gianfranco.dallabetta@unitn.it

Cinzia Da Via
University of Manchester, UK

Sebastian Grinstein, Andrea Micelli, Shota Tsiskaridze
Institut de Fisica d'Altes Energies (IFAE) and ICREA, Universitat Autonoma de Barcelona (UAB), Spain

Philippe Grenier
SLAC National Accelerator Laboratory, USA

Giovanni Darbo, Claudia Gemme
INFN Genova, Italy

Maurizio Boscardin
Fondazione Bruno Kessler, Trento, Italy

Giulio Pellegrini
Centro Nacional de Microelectronica, CNM-IMB (CSIC), Barcelona, Spain

Sherwood Parker
University of Hawaii, USA

Owing to their unique architecture, that allows the inter-electrode distance to be decoupled from the substrate thickness, 3D silicon sensors are intrinsically radiation hard devices. As such, they are suited to the demanding specifications of experiments at the High Luminosity LHC. The ATLAS Insertable B-Layer (IBL) project has represented a first important benchmark for 3D sensor technology. Owing to a joint effort of research institutes and processing facilities within the ATLAS 3D Sensor Collaboration, 3D pixel sensors compatible with the FE-I4 read-out chip and meeting the IBL specifications have been successfully produced. Selected results from the laboratory characterization and beam tests of irradiated 3D sensor assemblies during the IBL qualification campaign are reported and discussed in this paper.

The 21st International Workshop on Vertex Detectors
16-21 September 2012
Jeju, Korea

[1] *Speaker*

PoS(Vertex 2012)014

1. Introduction

A great deal of R&D activities have been carried out in the past decade concerning the radiation hardness of particle physics sensors in view of the High Luminosity (HL) LHC upgrades, where the innermost layers of pixel detectors will have to withstand radiation fluences in excess of 10^{16} 1-MeV equivalent neutrons (n_{eq}) cm^{-2} [1]. Among the different approaches so far investigated, which involve new materials, fabrication technologies, sensor designs and operational conditions, 3D silicon sensors represent one of the most promising options. 3D sensors, first proposed by S. Parker and collaborators in 1997 [2], consist of an array of n- and p-type columnar electrodes etched perpendicularly to the sensor surface and penetrating deeply through the substrate. By doing so, the signal charge, which is proportional to the substrate thickness, is decoupled from the charge collection process, which depends on the electrode distance. Since the latter is defined only by the sensor layout, it can be made very short (in the order of a few tens of microns), thus allowing for low depletion voltage and short charge collection time while keeping the active thickness unaltered. Most of all, charge trapping effects, which represent the ultimate limit to sensor performance at radiation fluences higher than 10^{15} n_{eq} cm^{-2} [3], can be effectively mitigated, since the electrode distance can be made comparable to the maximum drift length of charge carriers [4].

Evidence of the excellent radiation tolerance of 3D sensors has been already reported in the past few years, as will be reviewed in the following, with reference to both full 3D sensors with active edges developed at the Stanford Nanofabrication Facility (SNF), and double-sided 3D sensors (3D-DDTC) from FBK (Trento, Italy) [5] and CNM (Barcelona, Spain) [6], which proved to yield comparable performance both before and after irradiation.

This paper is organized as follows: in Section 2, earlier results from irradiated 3D sensors are recalled; in Section 3, the R&D activities aimed at the ATLAS Insertable B-Layer (IBL) [7], [8] are reviewed, with emphasis on the laboratory and beam test results obtained from irradiated 3D pixel sensors assemblies. Conclusions are drawn in Section 4.

2. Earlier results from irradiated 3D sensors

The first radiation hardness tests on 3D sensors from SNF are described in [9]: detectors irradiated with 24 GeV/c and 55 MeV protons at different fluences up to 10^{15} cm^{-2} were shown to yield a low depletion voltage, in the order of 100 V, and a leakage current in good agreement with expectations. The most significant result in terms of functional performance obtained with 3D sensors from SNF has been reported in [10]: a remarkably high signal efficiency (defined as the ratio of the signal amplitude after irradiation and before irradiation) of 66% was measured with an IR laser setup on 3D diode detectors irradiated with neutrons up to a 8.6×10^{15} n_{eq} cm^{-2} and read-out with a fast transimpedance amplifier.

As far as 3D-DDTC sensors are concerned, the charge collection performance after irradiation of the first samples made at FBK was limited by the non-optimized column depth, which resulted in the presence of low field regions. Nevertheless, pixel sensor assemblies using

the ATLAS FE-I3 read-out chip have shown signal efficiency values in response to radioactive sources of 76% and 64% at 1×10^{15} n_{eq} cm^{-2} and 2×10^{15} n_{eq} cm^{-2}, respectively [11]. The same sensors have been further characterized in several beam tests with good results in terms of hit efficiency, charge collection, and charge sharing up to a fluence of 1×10^{15} n_{eq} cm^{-2} [12].

Owing to an optimized column overlap, 3D-DDTC sensors made at CNM have shown excellent results after irradiation up to much larger fluences. In particular, sensors in the strip configuration (both p-on-n and n-on-p, with a distance of about 56 μm between n- and p-electrodes) read-out with the Alibava system, are fully efficient after 2×10^{15} n_{eq} cm^{-2} [13]. Moreover, due to a charge multiplication effect, the signal efficiency is still 70% at 350 V after a fluence of 2×10^{16} n_{eq} cm^{-2} [13]. Note that charge multiplication effects have been observed in 3D-DDTC strip sensors also at lower voltages (in the order of 200 V) after lower radiation fluences (starting from 5×10^{14} n_{eq} cm^{-2}) [13], [14], and are likely enhanced by the high electric field values at column tips, as suggested by TCAD simulations [15].

3. The ATLAS IBL campaign

Since 2009, the activities of the ATLAS 3D Sensor Collaboration have been mainly oriented to the ATLAS IBL, which gave a fundamental boost to the progress with 3D sensors in several respects [16]. On one hand it pushed 3D sensor technology to rapidly evolve and reach its maturity, eventually leading to the first production of 3D sensors ever made [17]. On the other hand, it called for an extensive experimental work on 3D pixel sensor assemblies both in laboratory and in beam tests, allowing for a deep insight into their performance after irradiation.

3.1 Sensor development

The four 3D processing facilities involved with the ATLAS 3D Sensor Collaboration (SNF, SINTEF, FBK, and CNM) agreed to combine their expertise in view of the IBL challenge. A common wafer design was used, aiming at full mechanical compatibility and equivalent functional performance of the 3D sensors to be produced, while maintaining the specific flavors of the different technologies [16]. The wafer layout includes eight pixel sensors compatible with the new read-out chip FE-I4 [18]. These sensors have a total area of ~4 cm^2 and contain 80×336 pixels. Each pixel has a size of 250 μm × 50 μm, with two read-out (n-type) columns, each one surrounded by four bias (p-type) columns at a distance of about 67 μm. Sensors feature a slim edge of ~200 μm in the direction parallel to the beam, and are fabricated on 230 μm thick, Float Zone, p-type silicon wafers, having a resistivity in the range from 10 to 30 kΩ cm. Columns are passing through for SNF, SINTEF, and FBK technologies, whereas for the CNM ones the column overlap is ~ 200 μm. More details on the sensor design and technology can be found in [16].

All processing facilities started the fabrication of IBL qualification batches with the common wafer layout in 2010. Due to their faster processing times, which was better suited to meet the tight IBL installation target of 2013 during the first long shut down of the LHC [8], only CNM and FBK were later involved in the sensor production [16],[17]. Results reported in this paper refer to 3D pixel sensors from the FBK and CNM qualification batches.

3.2 Experimental activities

Several sensors were bump bonded to the FE-I4 read-out chip at IZM (Berlin, Germany). The assemblies have been tested both before and after irradiation in laboratory and test beams. A comprehensive review of the results can be found in [19]. Here we will focus on the performance of the irradiated samples. Note that the specifications for the IBL include: operation at -15°C, a maximum leakage current of 100 nA/pixel (due to the FE-I4 compensation specification), a maximum power dissipation of 200 mW cm^{-2}, and an in-time hit efficiency > 97% after a benchmark fluence of 5×10^{15} n_{eq} cm^{-2} at 15° track inclination angle [19].

Several sensors from FBK and CNM were irradiated with protons and neutrons up to the IBL maximum fluence (6×10^{15} n_{eq} cm^{-2}). Proton irradiation was carried out at the KIT cyclotron (Karlsruhe, Germany) with 25 MeV protons. It should be mentioned that the estimated Total Ionizing Dose was ~ 750 Mrad, much higher than the IBL requirement of 250 Mrad, for which the FE-I4 chip is qualified. Neutron irradiation was carried out at the TRIGA reactor (Ljubljana, Slovenia). All assemblies were annealed for 120 minutes at 60°C before testing.

Beam tests were performed with 120 GeV pions at CERN SPS and with 4 GeV positrons at DESY, using the high resolution EUDET telescope and four scintillators as a trigger. Several DUTs (irradiated and not) were distributed in different beam test periods, always including a planar sensor as a reference. Measurements were taken with both particle tracks perpendicular to the sensors, and non-perpendicular incidence tracks to emulate the IBL geometry. More details on the measurement setups can be found in [19].

3.3 Results and discussion

After irradiation, electrical tests were performed first on the assemblies. As an example, Fig.1 shows the leakage current and power dissipation as a function of fluence at different temperatures for CNM and FBK sensors irradiated with protons. At 5×10^{15} n_{eq} cm^{-2}, the values measured at -15°C are about a factor of 10 lower than the IBL specification for both the leakage current (~10 nA/pixel vs 100 nA/pixel) and the power dissipation (~15 mW cm^{-2} vs 200 mW cm^{-2}). Similar results have been obtained on the neutron irradiated samples.

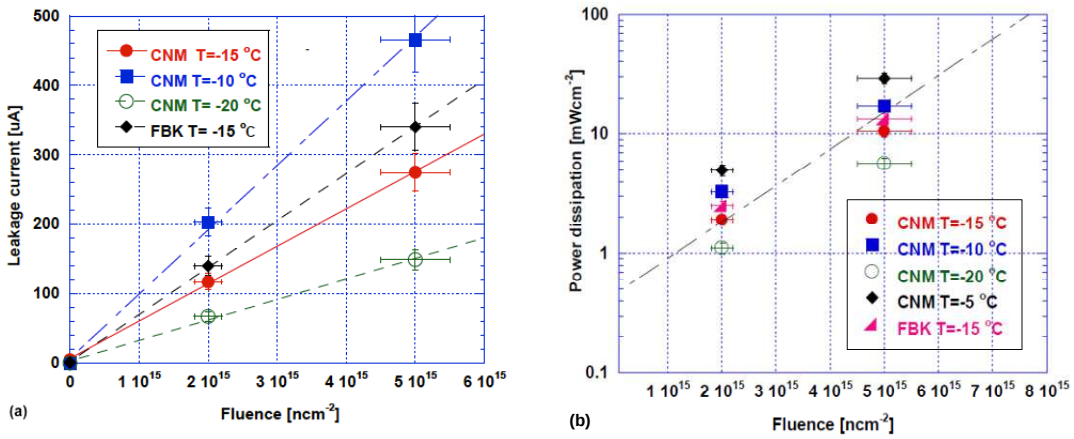

Figure 1 (a) Leakage current, and (b) power dissipation vs fluence at different temperatures for CNM and FBK pixel sensor assemblies irradiated with 25 MeV protons.

The sensor leakage current was found to be stable with time. As an example, Fig.2 shows data relevant to a CNM sensor irradiated with protons at 5×10^{15} n_{eq} cm^{-2} and biased at 144 V. The temperature was measured using a PT 1000 resistor glued on the aluminium plate in contact with the read-out chip. Different measurements were taken in order to account for the temperature variation induced by the heat transfer from the read-out chip.

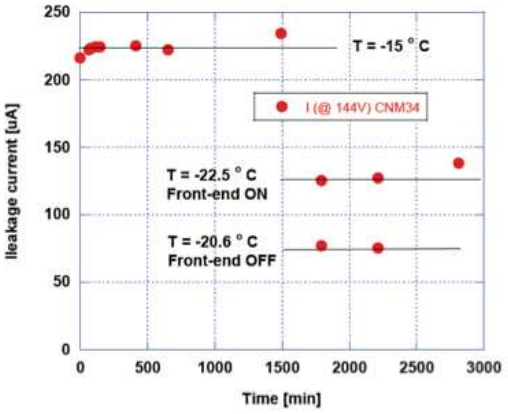

Figure 2 Stability of leakage current with time for a CNM pixel sensor assembly irradiated with protons at 5×10^{15} n_{eq} cm^{-2}.

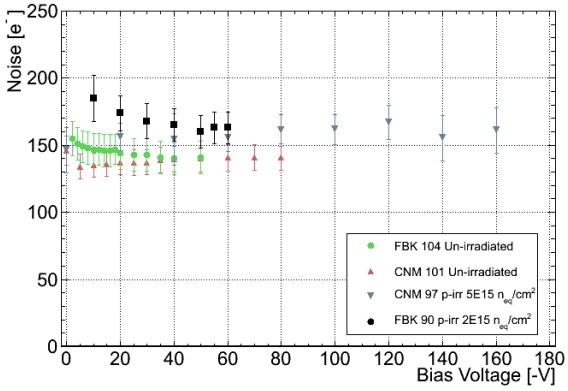

Figure 3 Noise vs bias voltage for different pixel sensor assemblies from CNM and FBK before and after proton irradiation.

Fig. 3 shows noise as a function of bias voltage (stopping at the breakdown voltage) for both non-irradiated and proton irradiated samples from CNM and FBK. Data have been measured using a calibration with a threshold of 3200 e^- and a Time-over-Threshold (ToT) of either 5 or 8 bunch crossings for a 20000 e^- signal. Noise is similar in CNM and FBK sensor and does not increase significantly after irradiation. In spite of the relatively high capacitance of 3D sensors (~200 fF per pixel), the noise figures are not far from those measured on planar sensor assemblies [19]. This remarkable result is due to the excellent performance of the FE-I4 chip, which also allows sensors to be operated with lower threshold values even after the largest radiation fluence. As an example, Fig.4 shows the 2D map and corresponding distribution of threshold and noise values in a CNM sensor irradiated at 5×10^{15} n_{eq} cm^{-2} and tuned at a threshold of 1300 e^-. A very good uniformity of the threshold is obtained, with a minor impact on noise.

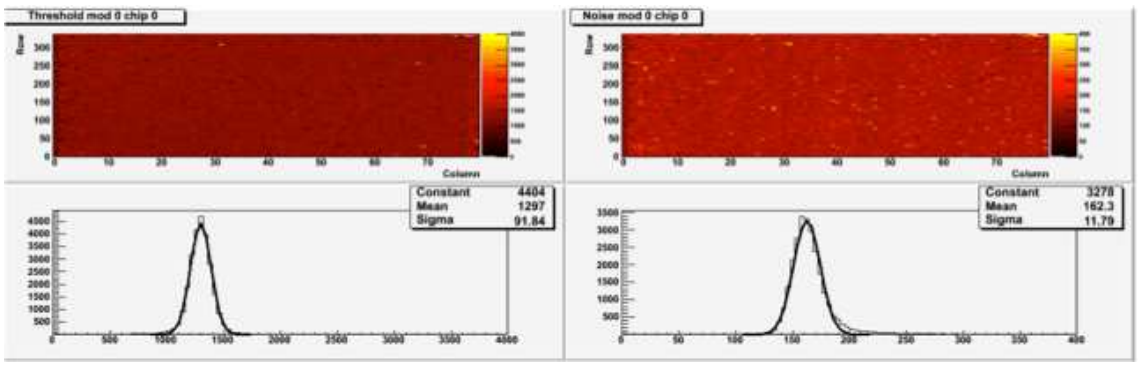

Figure 4 Threshold (left) and noise (right) 2D map and distribution for a CNM pixel sensor assembly irradiated with protons at 5×10^{15} n_{eq} cm^{-2}. Units for horizontal axes of distributions are e^-.

Fig. 5 shows the collected charge (most probable value of the spectrum) as a function of bias voltage in different sensors exposed to a ^{90}Sr source. Before irradiation full charge collection (~10 ToT) is achieved already at low voltage (~10 V) for the FBK sensor and at a slightly higher voltage for the CNM sensor. This difference is to be ascribed to the lower depletion voltage in FBK sensors thanks to the passing-through columns, an effect that is also evident after irradiation. Provided that the voltage is high enough to ensure depletion, sensors are still able to collect a large amount of charge even after large radiation fluences. Comparable charge collection performance is achieved for FBK and CNM sensors, but for the previously mentioned effect related to column depth which results in a voltage shift. The trend in the signal efficiency (higher than 80% at 2×10^{15} n_{eq} cm^{-2} and higher than 60% at 5×10^{15} n_{eq} cm^{-2}) is consistent with the analytical predictions based on the inter-electrode spacing and the effective drift length caused by charge trapping at the considered fluences [17]. For the FBK sensors, TCAD simulations have been performed with Synopsys Sentaurus, incorporating the "Perugia" trap model [20] modified as described in [21] to account for radiation damage. Simulated data are also shown in Fig. 5: the agreement with measurements is excellent for the non-irradiated sensor and good enough for the irradiated one, considering the uncertainties in the calibration, irradiation fluence, and annealing conditions.

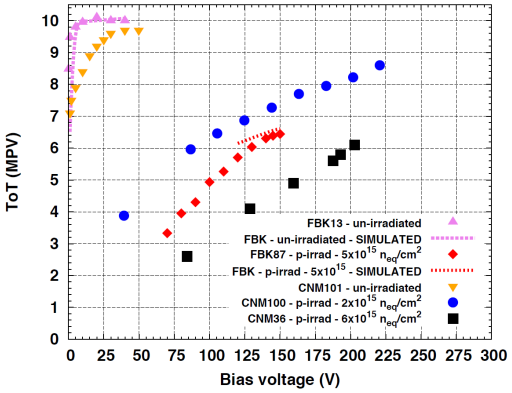

Figure 5 Collected charge (in units of ToT) vs bias voltage, measured for selected non-irradiated and irradiated FBK and CNM sensors exposed to a ^{90}Sr source. Simulated data are also shown for FBK sensors.

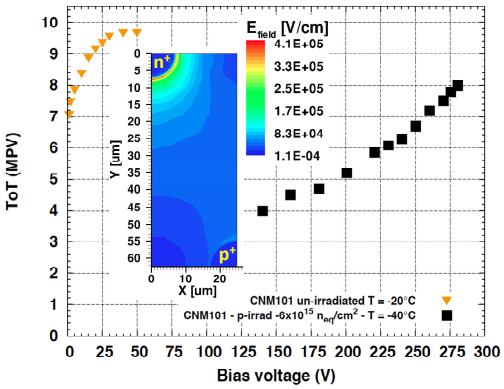

Figure 6 Collected charge (in units of ToT) vs bias voltage, measured at -40°C on CNM101 sensor exposed to a ^{90}Sr source. A 2D map of the electric field at 280 V at a depth of 205 μm, corresponding to the n^+ column tip, is shown in the inset.

Fig. 6 shows data relevant to the CNM sensor irradiated at 6×10^{15} n_{eq} cm^{-2}, which was re-measured at -40°C in order to extend the operation voltage range while trying to keep the noise at an acceptable level. The goal of this test was to explore charge multiplication effects possibly occurring at high voltage, as also observed in 3D strip sensors from CNM [13]. In fact, the large collected charge value (8 ToT) reached at 280 V and the fact the non-saturating trend in collected charge values are compatible with the presence of impact ionization effects. Most likely, this is due to multiplication of electrons close to the read-out electrodes and particularly at the column tips, where the electric field peak is more pronounced and exceeds 4×10^5 V/cm, as confirmed by TCAD simulations incorporating the bulk trap model (see inset in Fig. 6). This value is high enough for the onset of charge multiplication. Nevertheless, this is a preliminary result that should be further assessed with both measurements and simulations.

Table 1 summarizes the most important results from the beam tests performed at CERN in 2011. Data are relevant to both non-irradiated and irradiated sensors measured in different conditions. Non-irradiated samples were measured with perpendicular tracks, and high efficiency was obtained already at low voltage. Note that due to the columnar electrodes 3D

sensors cannot be fully efficient with perpendicular tracks. In this respect, CNM sensors perform better than FBK ones because they can collect charge from the regions between the column tips and the opposite surface, whereas in FBK sensors the passing through columns are dead regions. The hit efficiency is generally very good also after irradiation and compatible with the IBL specification. As expected from the poor electrode response, the hit efficiency is generally better for inclined tracks, but other aspects should be carefully considered, in particular the threshold value and the bias voltage. Efficiency losses derive from insufficient charge collection due to poor (or null) electrode response, low field regions and charge sharing at the pixel boundaries and especially at the corners. In all cases a lower threshold is useful, whereas the increase of bias voltage is fundamental to improve the efficiency from those regions close to p-type (bias) electrodes where the electric field is lower and charge sharing more pronounced. As can be seen from Table 1, increasing the bias voltage from 140 V to 160 V while reducing the threshold to 1500 e^- allowed for a significant increase of the hit efficiency, making it compatible with the IBL specifications (compare e.g., CNM34 at 15° to CNM97, and FBK87 to FBK11).

Sensor ID	**Bias (V)**	**Tilt Angle (°)**	**Irradiation**	**Fluence (n_{eq} cm^{-2})**	**Threshold (e^-)**	**Hit Efficiency (%)**
CNM55	20	0	No	-	1600	99.6
FBK13	20	0	No	-	1500	98.8
CNM34	140	0	25 MeV protons	5×10^{15}	1500	97.6
CNM34	160	0	25 MeV protons	5×10^{15}	1500	98.1
CNM97	140	15	25 MeV protons	5×10^{15}	1800	96.6
CNM34	160	15	25 MeV protons	5×10^{15}	1500	99.0
CNM81	160	0	Reactor neutrons	5×10^{15}	1500	97.5
FBK90	60	15	25 MeV protons	2×10^{15}	3200	99.2
FBK87	140	15	25 MeV protons	5×10^{15}	2000	95.6
FBK87(*)	160	15	25 MeV protons	5×10^{15}	1500	98.2

Table 1 Summary of the main results from the 2011 beam tests at CERN. (*) Results relevant to FBK87 sensor have been obtained from a beam test at DESY in April 2012. All results have been obtained with a tuning of 10 ToT at 20 ke$^-$ signal.

The beneficial effects of higher bias voltage on the efficiency can be better appreciated from Fig.7, which refers to sensor CNM34 as measured in the beam test using perpendicular tracks. At 100 V (Fig.7b), all electrodes are clearly visible from the 2D maps as low efficiency spots, and the total efficiency is 96.6%. Increasing the voltage improves the efficiency in the critical regions. In particular, at 160 V (Fig.7e) the inefficiencies related to the n-type columns disappear, because of the enhanced charge collection from the regions underneath the read-out (n-type) column tips. Increasing the voltage to 180 V further improves the efficiency, but this comes at the expense of a significant increase in the fraction of noisy pixels (~1% at 160 V,

~8% at 180 V [22]), due to high leakage current. Thus, for these sensors 160 V represents the upper limit of the bias voltage for low noise operation. Future applications of 3D sensors at HL LHC will require a higher breakdown voltage, which could otherwise become the limiting factor after very large radiation fluences and prevent the sensor to be properly biased to a value ensuring full lateral depletion and sufficiently high electric field. While different 3D configurations with shorter inter-electrode distances are more appropriate for very large radiation fluences [10], the sensor design and fabrication technology should be optimized in order to extend the operation voltage range after irradiation [23].

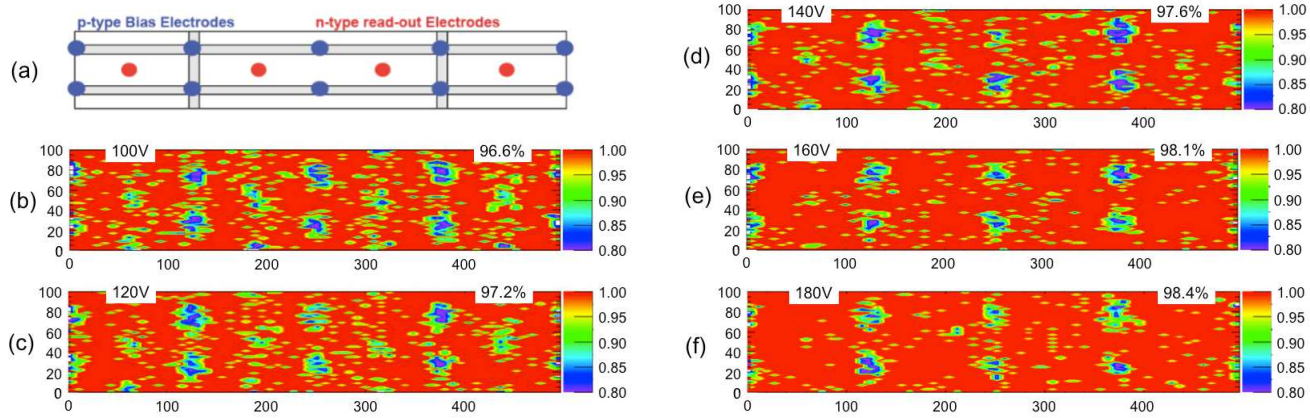

Figure 7 Cell hit efficiency maps: a) sketch of the basic cell layout; (b)-(f) 2D efficiency maps at different bias voltages for the CNM34 sensor operated at a threshold of 1500 e^- using normal incident tracks. All dimensions are in microns.

The hit efficiency of the edge pixels allowed the size of the inactive area at the sensor edge to be estimated. As an example, Fig.8 shows the layout of the edge region in an FBK sensor irradiated with protons at 2×10^{15} n_{eq} cm^{-2} and the one-dimensional efficiency projection onto the long pixel direction extracted from the hit efficiency map and fit with an s-curve function. The slim edge design in FBK sensors has a 200 µm ohmic fence (black circles in Fig. 8) termination extending over the edge pixels [24], but a few µm of residual from the scribe-lines after cut are also present. In Fig.8, the active area is shown to extend to about 20 µm over the edge pixel making the inactive area also approximately 200 µm at 50% efficiency. Similar results for the edge efficiency have been obtained for CNM sensors and at larger radiation fluences [19].

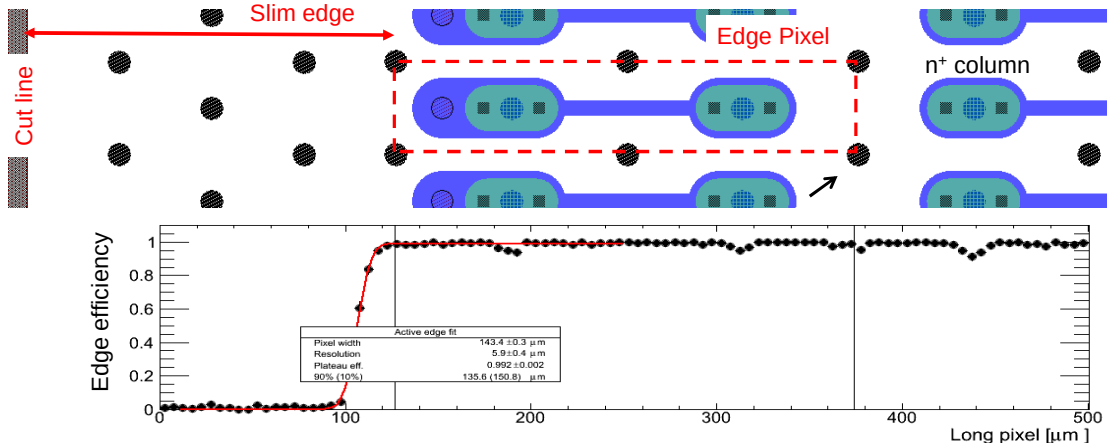

Figure 8 Edge efficiency measurement for the FBK90 sensor operated at 60V bias using 15° inclined tracks. The edge layout and the 1D efficiency projection onto the long pixel direction are shown.

4. Conclusions

We have reported on selected results from irradiated 3D pixel sensors from FBK and CNM oriented to the ATLAS IBL. Several samples bump bonded to the FE-I4 read-out chip have been irradiated with protons and neutrons up to large fluences (6×10^{15} n_{eq} cm^{-2}) and characterized in laboratory and beam tests at CERN and at DESY. While confirming that 3D sensors have good charge collection performance after irradiation and that they safely meet the IBL specifications, test results provided deep insight into the sensor behavior as well as useful indications for the proper choice of the bias voltage in order to obtain a high hit efficiency. 3D sensors irradiated at the IBL benchmark fluence of 5×10^{15} n_{eq} cm^{-2} and operated at 160 V bias have a hit efficiency better than 98% at 15° track inclination angle with a power dissipation lower than 20 mW cm^{-2} at -15°C. Low threshold operation (down to 1300 e^-) with acceptable noise occupancy after the maximum fluence has also been possible owing to the remarkably good performance of the FE-I4 read-out chip. Finally, the edge efficiency tests confirm the layout-based expectation of about 200 μm of inactive region at the sensor edge.

Acknowledgements

This work has been partially funded by: i) the Spanish Ministry of Education and Science through the Particle Physics National Program FPA2010-22060-C02-00 and co-financed with FEDER funds; (ii) the Provincia Autonoma di Trento through the Project MEMS2; (iii) the Italian National Institute for Nuclear Physics (INFN) through the Projects TRIDEAS (CSN5) and ATLAS (CSN1); (iv) the US Department of Energy through the contract DE-AC02-76-SFO0515.

Irradiation studies at the cyclotron in Karlsruhe (Germany) and the TRIGA reactor in Ljubljana (Slovenia) have received funding from the European Commission under the FP7 Research Infrastructures project AIDA, grant agreement no. 262025.

The authors are grateful to all members of the ATLAS 3D Sensor Collaboration for their support to this project.

References

[1] G. Casse (on behalf of the CERN RD50 Collaboration), *Overview of the recent activities of the RD50 collaboration on radiation hardening of semiconductor detectors for the sLHC, Nucl. Instrum. Methods A* **598** (2009) 54.

[2] S. Parker, et al., *3D - A proposed new architecture for solid-state silicon detectors, Nucl. Instrum. Methods A* **395** (1997) 328.

[3] G. Kramberger, et al., *Impact of annealing of trapping times on charge collection in irradiated silicon detectors, Nucl. Instrum. Methods A* **579** (2007) 762.

[4] C. Da Via, S.J. Watts, *The geometrical dependence of radiation hardness in planar and 3D silicon detectors, Nucl. Instrum. Methods A* **603** (2009) 319.

[5] A. Zoboli, et al., *Double-Sided, Double-Type-Column 3-D Detectors: Design, Fabrication, and Technology Evaluation, IEEE Trans. Nucl. Sci.* **55(5)** (2008) 2775.

[6] G. Pellegrini, et al., *First double-sided 3-D detectors fabricated at CNM-IMB, Nucl. Instrum. Methods A* **592** (2008) 38.

[7] M. Capeans, et al. (The ATLAS Collaboration), *ATLAS Insertable B-Layer Technical Design Report*, CERNLHCC-2010-013; ATLAS-TDR-019.

[8] G. Darbo, M. Nessi (The ATLAS Collaboration), *ATLAS Insertable B-Layer Technical Design Report Addendum*, CERN-LHCC-2012-009; ATLAS-TDR-019-ADD-1.

[9] S. I. Parker, C. J. Kenney, *Performance of 3-D architecture silicon sensors after intense proton irradiation, IEEE Trans. Nucl. Sci.* **48(5)** (2001) 1629.

[10] C. Da Via, et al., *3D active edge silicon sensors with different electrode configurations: Radiation hardness and noise performance, Nucl. Instrum. Methods* A **604** (2009) 505.

[11] A. La Rosa, et al., *Characterization of proton irradiated 3D-DDTC pixel sensor prototypes fabricated at FBK, Nucl. Instrum. Methods A* **681** (2012) 25.

[12] A. Micelli, et al., *3D-FBK pixel sensors: Recent beam tests results with irradiated devices, Nucl. Instrum. Methods A* **650** (2011) 150.

[13] M. Koehler, et al., *Comparative measurements of highly irradiated n-in-p and p-in-n 3D silicon strip detectors, Nucl. Instrum. Methods A* **659** (2011) 272.

[14] A. Zoboli, et al., *Functional Characterization of 3D-DDTC Detectors Fabricated at FBK-irst*, in Conference Record of *2008 IEEE Nuclear Science Symposium*, N34-4.

[15] G. Giacomini, et al., *Simulations of 3D detectors*, in Proceedings of *20th International Workshop on Vertex Detectors* PoS(Vertex2011) 025.

[16] C. Da Via, et al., *3D Silicon Sensors: Design, Large Area Production and Quality Assurance for the ATLAS IBL Pixel Detector Upgrade, Nucl. Instrum. Methods A* **694** (2012) 321.

[17] C. Da Via, et al., *3D active edge silicon sensors: Device processing, yield and QA for the ATLAS-IBL production, Nucl. Instrum. Methods A* **699** (2013) 18.

[18] M. Garcia-Sciveres, et al., *The FE-I4 Pixel Readout Integrated Circuit, Nucl. Instrum. Methods A* **636** (2011) S155.

[19] The ATLAS IBL Collaboration, *Prototype ATLAS IBL Modules using the FE-I4A Front-End Readout Chip, JINST* **7** (2012) P11010.

[20] M. Petasecca, et al., *Numerical Simulation of Radiation Damage Effects in p-Type and n-Type FZ Silicon Detectors, IEEE Trans. Nucl. Sci.* **53(5)** (2006) 2971.

[21] D. Pennicard et al., *Simulations of radiation-damaged 3D detectors for the Super-LHC, Nucl. Instrum. Methods A* **592** (2008) 16.

[22] S. Grinstein, *Overview of the ATLAS Insertable B-layer (IBL) project, Nucl. Instrum. Methods A* **699** (2013) 61.

[23] M. Povoli, et al., *Layout and Process Improvements to Double-Sided Silicon 3D Detectors Fabricated at FBK*, in Conference Record of *2012 IEEE Nuclear Science Symposium*, paper N14-204.

[24] M. Povoli, et al., *Slim edges in double-sided silicon 3D detectors, JINST* **7** (2012) C01015.